Biomed Microdevices (2011) 13:315–323
DOI 10.1007/s10544-010-9495-1

A microfluidic respiratory assist device with high gas permeance for artificial lung applications

Tatiana Kniazeva · James C. Hsiao · Joseph L. Charest · Jeffrey T. Borenstein

Published online: 27 November 2010

Abstract One of the principal challenges in artificial lung technology has been the ability to provide levels of oxygen and carbon dioxide exchange that rival those of the natural human lung, while mitigating the deleterious interaction between blood and the surface of the synthetic gas exchange membrane. This interaction is exacerbated by the large oxygenator surface area required to achieve sufficient levels of gas transfer. In an effort to address this challenge, microfluidics-based artificial lung technologies comprising stacked microchannel networks have been explored by several groups. Here we report the design, fabrication and initial testing of a parallel plate multilayered silicone-based microfluidic construct containing ultrathin gas exchange membranes, aimed at maximizing gas transfer efficiency while minimizing membrane-blood contact area. The device comprises a branched microvascular network that provides controlled wall shear stress and uniform blood flow, and is designed to minimize blood damage, thrombosis and inflammatory responses seen in current oxygenators. Initial testing indicates that flow distribution through the multilayer structure is uniform and that the thin membrane can withstand pressures equivalent to those expected during operation. Oxygen transfer using phosphate buffered saline as the carrier fluid has also been assessed, demonstrating a sharp increase in oxygen transfer as membrane thickness is reduced, consistent with the expected values of oxygen permeance for thin silicone membranes.

Keywords Microfluidics · Artificial organs · PDMS · Oxygen transport · Vascular

T. Kniazeva · J. C. Hsiao · J. L. Charest · J. T. Borenstein (✉)
Charles Stark Draper Laboratory,
Cambridge, MA, USA
e-mail: jborenstein@draper.com

1 Introduction

In spite of significant advances in artificial lung technology, the unique architecture and extraordinary efficiency of the human lung has yet to be paralleled by engineered systems. When lung function is compromised due to disease, injury or prenatal complications, a lung-assist device incorporating a membrane oxygenator may be needed to maintain the blood gas levels necessary for survival. Cardiopulmonary support devices are widely used for surgical support and ExtraCorporeal Membrane Oxygenator (ECMO) machines may be appropriate for critical and emergency care situations. However, there is a need for improved membrane oxygenators that will provide high gas transfer while minimizing the risks posed to ECMO patients, especially neonatal patients who are more vulnerable to hemorrhage and other complications and may require ECMO support for an extended period of time.

Most artificial lung devices used today are comprised of a series of hollow porous fiber bundles inside a hard-shelled jacket. Oxygen is introduced intraluminally through the fibers and diffused into venous blood flowing around the fibers, often forcing turbulence for maximum membrane exposure (Hammon 2008). The effective gas transfer area of the membrane ranges between 0.5 to 4.5 m^2 (High et al. 2000; Dierickx et al. 2001), resulting in a surface area to volume ratio 10 times less than the natural lung, and a gas diffusion distance of 10–30 μm, far greater than the 1 μm alveolar-blood membrane thickness in the lung (Federspiel and Henchir 2004). Though the fibers are made of a hydrophobic polymer to reduce blood plasma leakage into the fiber wall, phospholipids, lipoproteins and proteins from the plasma inevitably penetrate the submicrometer pores over time, reducing the membrane gas permeability, which can cause device failure within days (Montoya et al. 1992; Federspiel and Henchir 2004). To prevent plasma

leakage, some ECMO membranes are coated with a thin non-porous polymer such as silicone (Shimono et al. 1997), which increases cost and reduces oxygen permeance of the membrane (Niimi et al. 1997). Adverse interactions between blood and the device tubing, made of polyvinylchloride (PVC), Tygon or silicone, increases the risk of thrombosis, requiring a high level of anticoagulant administration, which can cause excessive bleeding and electrolyte-related imbalances in the patient (Stiller et al. 2004; Brand 2009). These risks are further exacerbated by larger priming volumes, resulting in increased blood-membrane interactions and hence the need for higher levels of anticoagulants. Due to limitations in the minimum achievable diameter and concomitant total surface area of the porous fibers, current ECMO devices require large priming volumes, with adult oxygenators requiring 220 to 560 mL (Hammon 2008) of blood, and neonatal machines requiring as much as 130 mL (Brand 2009). Additionally, the non-physiological blood flow pathways in current ECMO machines generate fluid forces that are largely unpredictable and uncontrolled. The resulting flow patterns can result in red blood cell (RBC) damage as well as inflammatory responses that increase morbidity and mortality in ECMO patients (Cook et al. 2002; Leverett et al. 1972; Hattler et al. 2002). By avoiding tortuous flow patterns, levels of shear stress can be predicted, regulated, and made consistent throughout an ECMO device.

Many of the limitations seen in current ECMO devices may be addressed by utilizing microelectromechanical systems (MEMS)-based microfabricated channels for blood transport. Because the blood-side passages in hollow fiber ECMO devices are 200–300 μm in diameter, compared to 5–10 μm for a capillary, transverse blood mixing is necessary to expose more RBCs to the gas-exchange surface of the membrane (Lee et al. 2008). By providing channels with depths smaller than traditional 200–300 μm diameter hollow fibers for blood to pass through, the MEMS-based designs can maximize RBC contact with the oxygen-rich fluid layer along the surface of the membrane, while regulating shear stresses within the fluid. Microchannels may be fabricated from poly(dimethylsiloxane) (PDMS) (Borenstein et al. 2002; Burgess et al. 2008), a silicone rubber material commonly used in microfluidic devices. PDMS has performed well in blood-contact applications, is highly gas-permeable, cost-efficient, and easy to handle, making it a suitable material for the fabrication of blood-flowing microchannels, as well as for producing non-porous membranes of varying thicknesses.

Early studies of oxygen diffusion through 125 μm and 50 μm slabs of PDMS containing single rounded microchannels of 25 μm and 10 μm diameters by Page et al. (1996, 1999) found that blood can be oxygenated to arterial levels in 0.8 and 0.2 s, respectively. Networks comprising numerous microchannels bonded to silicone membranes have been incorporated in both cellularized (Borenstein et al. 2002; Burgess et al. 2008; Huh et al. 2010) and acellular devices (Burgess et al. 2008; Lee et al. 2008) to explore the use of microfluidics for artificial vasculatures for organ assist devices. These studies demonstrated that oxygen transport exhibits a dependence on the residence time (Page et al. 1999), channel height and width (Lee et al. 2008), and membrane thickness (Burgess et al. 2008). In comparing transport in 12 μm and 25 μm deep rectangular microchannels, Lee et al (2008) found that the deeper channels allowed for longer blood channels that maintained a suitable blood side pressure drop of 15 mm Hg and an acceptable trauma factor. The trauma factor depends on shear stress and exposure time, and must be lower than zero in order to avoid blood trauma (Mockros and Cook 2002). Burgess et al (2008) evaluated the effect of silicone membrane thickness on oxygen transfer into static fluid, and found that oxygen permeance increased with decreasing thickness of the silicone membrane, as expected based on previous reports in the literature (Yasuda 1975). The gas permeance of a membrane is not the only governing factor for gas exchange into a flowing medium; the diffusional boundary layers that are formed along the membrane and other fluid dynamic considerations play a crucial role in the gas exchange of an artificial lung device. Though the aforementioned investigations have provided a general understanding of various design aspects of a membrane oxygenator, there is yet to be a single model that incorporates fluid dynamic control, membrane permeance, and channel geometry to oxygenate blood to arterial levels.

In the present work, we have designed and constructed a parallel plate multilayered silicone-based microfluidic device which contains branched microvascular networks separated from oxygen channels by thin non-porous PDMS membranes with high gas permeance. The network design utilizes a biomimetic flow pattern in small channels to reduce both the fluid forces on the blood in the channels and the overall volume of the device. The device maximizes gas transfer efficiency by incorporating an ultrathin membrane with high oxygen permeance and by providing a membrane-blood contact area sufficient for high levels of oxygenation without the need for large blood prime volumes. Because the membrane is thinner than those generally seen in ECMO devices, it is more gas permeable and will require less surface area for equivalent oxygen transfer. Reduced membrane area is also expected to reduce the complications associated with blood-membrane interactions, potentially lowering the tendency for thrombosis and inflammatory responses.

2 Methods and materials

2.1 Device design

The overall structure of our device was based on a scaling strategy in which individual blood-gas subunits could be stacked to increase the capacity of the device. Each blood-gas subunit represents a bilayer consisting of a vascular microchannel network for blood flow separated by a thin membrane from an oxygen channel. With an arrangement of alternating vascular and oxygen channels, the overall device utilizes the high surface area to volume ratio of each vascular layer in a larger overall network, allowing a higher volume of blood to be processed in one cycle. Each vascular microchannel network receives oxygen from oxygen channels situated above and below it, doubling the transfer capacity of the device.

The vascular microchannel networks were designed to eliminate areas of disturbed blood flow by implementing a series of bifurcating microchannels of varying widths and lengths that mimic the scaling laws seen in physiologic vasculature (Borenstein 2009, Borenstein et al. 2002). By creating a fluid path that incorporates smooth bifurcations and uniform fluid distribution, the wall shear stress along the channel is more controlled (Weinberg et al. 2004) when compared to typical microfluidic devices or blood-flowing devices using large, open manifolds. A computational model of the expected wall shear stress distribution in a portion of the vascular network is shown in Fig. 1(a). The specific proportions of the multiple-width bifurcating channel network were selected to mimic design rules for natural vasculature and ensure smooth transitions (Emerson et al. 2006). These design rules are based upon principles such as Murray's Law, which states that the sum of the cubes of the diameters of two daughter vessels at a bifurcation is equal to the cube of the diameter of the parent vessel (Murray 1926; Borenstein et al. 2010; Lim et al. 2003). Other physiological considerations such as the nature of the velocity profile, smoothness of blood flow, and control of oxygen distribution are also reflected in the design of the bifurcation angles and channel dimensions. The mask design for the vascular network is shown in Fig. 1(b).

For ease of fabrication, channels with rectangular cross sections were chosen for the vascular microchannel network. New fabrication techniques capable of producing rounded channels have recently been developed (Borenstein et al. 2010; Camp et al. 2008; Wang et al. 2007; Seo et al. 2004) and may have beneficial effects regarding blood flow. These techniques may be useful in future generations of artificial lung devices, but will require new approaches for integration with the membrane. Rectangular channels in the current device were of varying widths but were designed to be 100 μm in depth throughout, in order to provide a small total volume for each channel and therefore reduce the diffusion distance required for oxygen and CO_2 transfer.

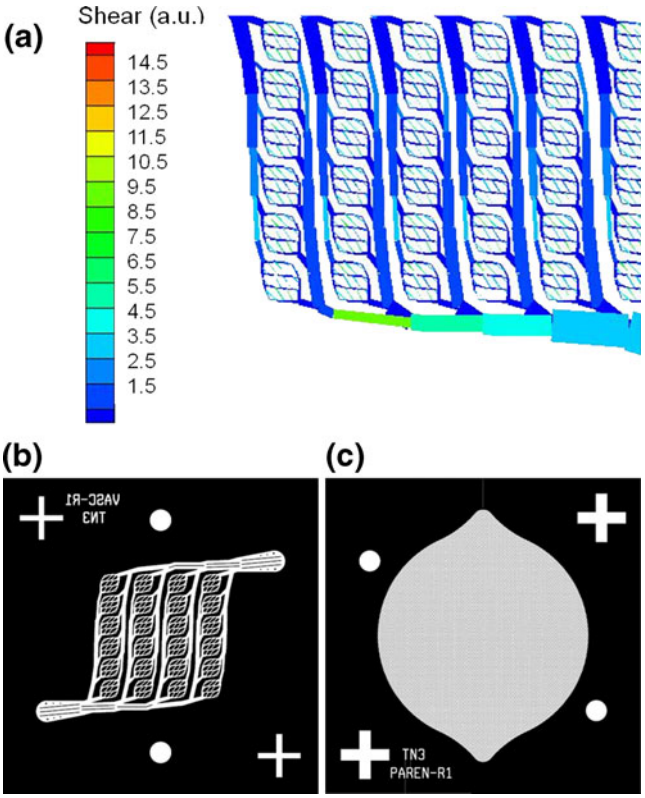

Fig. 1 **(a)** A computational model of wall shear stress for whole blood rheology, with 80 mm Hg inlet pressure. The design is intended to establish a constant level of shear stress throughout the microfluidic network. Wall shear stress (in arbitrary units) is minimal for this design throughout the microfluidic network. Layout of mask designs for vascular (**b**) and oxygen (**c**) channel molds. Working medium flows in through access ports at the upper right, distributes throughout the microchannels, and exits through another access port at the lower left. Similarly, the oxygen channel features an inlet at the top, and outlet at the bottom of the channel. The two mask designs feature alignment marks in the corners, as well as circular marks to indicate hole punching sites for interlayer fluid exchange

The oxygen channel, depicted in Fig. 1(c), was designed to maximize oxygen contact area with the membrane. The channel has a total surface area of 252.97 mm^2, which completely overlaps and extends beyond the 85.23 mm^2 membrane surface area of the vascular network. For structural integrity, the oxygen channel includes 100 μm diameter posts throughout, spaced 100 μm apart vertically and 246 μm apart horizontally. These posts maintain the vertical gap between the oxygen channel bottom surface and the membrane. Similarly, 100 μm ribs were added to the vascular inlet and outlet ports, to avoid the possibility of membrane collapse in the wide vascular channels.

2.2 Fabrication of PDMS devices

2.2.1 Casting the channel layers

The channel molds were built using MEMS fabrication technology, as previously reported for several other artificial organ applications (Borenstein et al. 2002; Leclerc et al. 2003). Using this method, silicon wafers were photolithographically patterned with the microchannel design using SU-8 negative photoresist and a mask with our specified design. These were then passivated with C_4F_8 and used as the mold from which our devices were cast. The entire fabrication process is outlined in Fig. 2.

The individual vascular and oxygen channel layers were made by mixing PDMS elastomer and curing agent (Sylgard 184, Dow Corning, Midland, MI) in a 10:1 ratio by mass. PDMS was poured into the silicon wafer molds, degassed for approximately 30 min under 23–25 in Hg, and placed in a 65°C oven to cure for a minimum of 3 h. All PDMS channel layers were 1 mm thick except for the layers that would be on the top and bottom of the overall device stack, which were cast to be 2.5 mm in thickness to accommodate tubing connections. After the PDMS was cured, each layer was cut to size along its edges. The bottom and top pieces were punched with a 1.5 mm biopsy punch for inlet and outlet tubing to be inserted.

2.2.2 Membrane fabrication and attachment

The PDMS membrane was made by spin-coating freshly-mixed PDMS onto an unpatterned, passivated silicon wafer

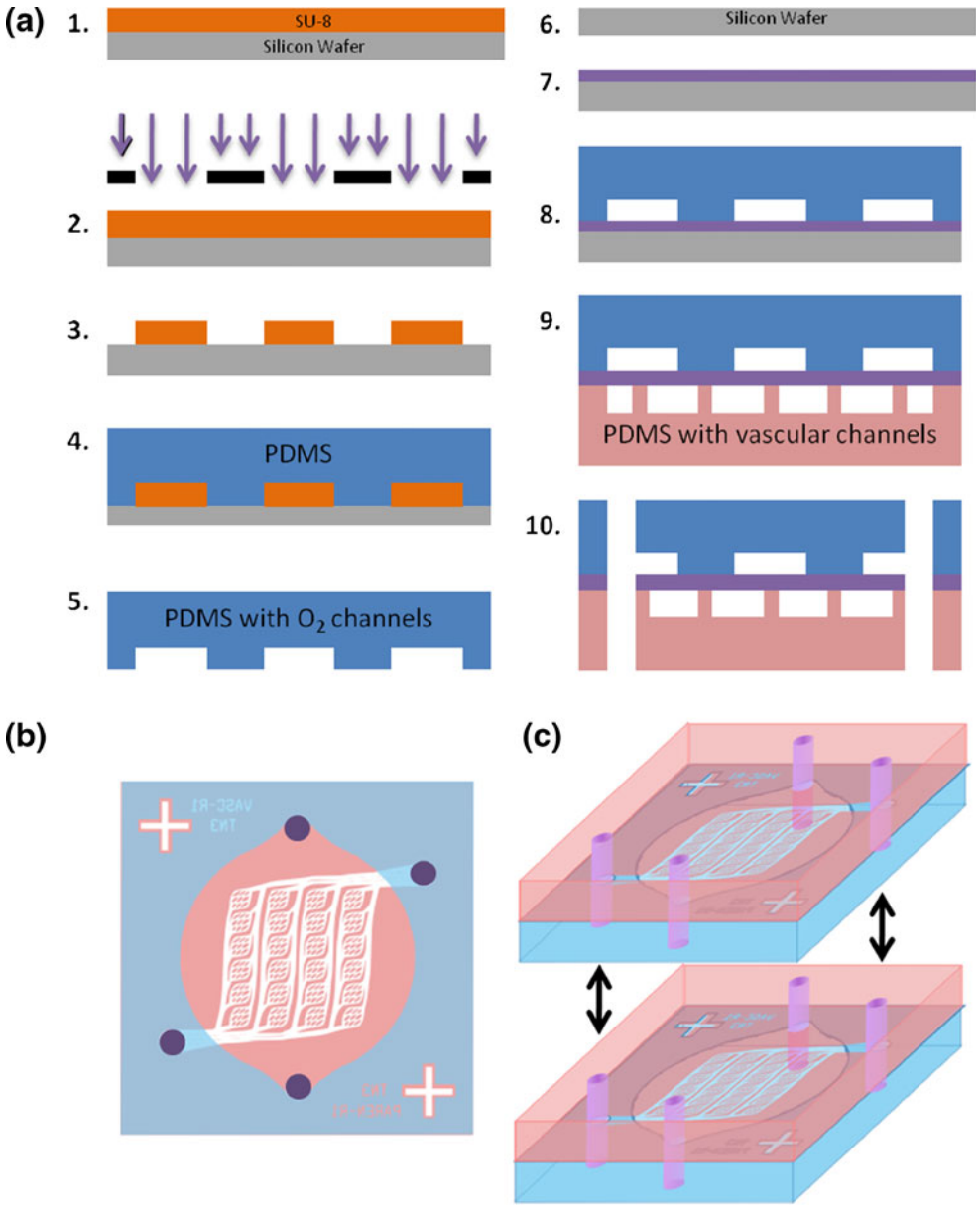

Fig. 2 (**a**) Fabrication process outline for creating each blood-gas bilayer subunit: SU-8 is patterned on a blank Si wafer to form the mold (1–3) for the PDMS channel pieces (4). Thin PDMS membrane is formed by spin-coating onto a passivated silicon wafer and plasma bonding to the oxygen channel piece. Next the channel piece and the membrane are plasma bonded to the vascular channel piece (9). Through-holes are punched through the assembled bilayer (10) (**b**) Top view of assembled bilayer outlines the overlapping area and through-hole punching sites at the inlets and outlets of each channel. **c** Schematic of two bilayers shows the alignment which enables fluid passage through each layer

using a Headway Research spin coater (Headway Research Inc, Garland, TX). A series of experiments were performed to determine the membrane thickness as a function of spin rate, and to determine how thin the membrane could be while maintaining necessary mechanical properties to withstand any pressure or flow changes. A curve was generated to characterize the dependence of membrane thickness on spin speed. The baseline membrane thickness we chose was about 11 μm, as confirmed by optical and SEM measurements of a cross-sectioned membrane, which was obtained by spinning at a rate of 5000 RPM with a ramp rate of 1000 rpm/sec, for a 60 s cycle. The wafers with freshly spun PDMS were placed in a 65°C oven to cure for a minimum of 45 min.

Membranes were attached to the oxygen channel layers using oxygen plasma treatment (March Plasma Systems, San Francisco, CA). The oxygen layers and the membrane (still attached to the unpatterned, passivated silicon wafer) were oxygen plasma treated at a pressure of 250 mTorr and a power of 100 W, for a total of 10 s. This treatment time was previously optimized to provide minimum plasma exposure while still forming a strong bond between the PDMS layers. After treatment, the oxygen channel layer was placed onto the membrane, any bubbles were removed, and the wafer was placed into the 65°C oven with a weight of 1–3 pounds placed on it. After approximately 30 min, the oxygen channel layers were lifted off of the wafer, along with the attached membrane. This was achieved by gently tracing the border of each thick PDMS piece with a sharp blade or very thin tweezers to cleave the attached membrane from the residual membrane on the wafer. Tweezers were then used to gently lift the PDMS oxygen channel layer, with the bonded membrane. To attach the vascular channel, the same plasma parameters were used to treat the opposite side of the membrane and the channel side of the vascular layer. After plasma treatment, the two layers were bonded using aligning marks on the face of each piece for precision. The complete bilayer was then placed in the 65°C oven under weights. After proper attachment, each central bilayer was punched with 4 through-holes in the inlets and outlets, which would allow both the oxygen and the vascular channels to connect with the next layer of their respective type. Gas exchange through each layer of the device was modeled using the polymer permeability constant equation (Yasuda 1975)

$$P = \frac{V \cdot D}{SA \cdot t \cdot \Delta P} \quad (1)$$

Here, the permeability constant of a material P, is used to describe the relationship between the volume of gas that will transfer through the polymer V, the polymer thickness D, surface area of gas exchange (SA), time (t), and the transmembrane pressure (ΔP). Using this equation, gas exchange through all layers other than the membrane was determined to be negligible.

2.2.3 General assembly

After the individual bilayer subunits were fabricated, they were attached to one another using the same oxygen plasma treatment parameters. Silastic Laboratory tubing (Dow Corning, Midland, MI) was connected to inlets and outlets of the oxygen channel. For the vascular inlets and outlets, polyetheretherketone (PEEK) tubing (Upchurch Scientific, Oak Harbor, WA) was used to minimize oxygen transfer through the tubing to reduce error in oxygen transfer measurements. Dow Corning 1044 Silicone Rubber RTV coating (Dow Corning, Midland, MI) was used to seal device-tubing interfaces to prevent leakage. For initial oxygen transfer testing, test devices were fabricated comprising two bilayers, stacked with the two vascular channels on the inside, and the two oxygen channels on the outside. Figure 3 depicts an assembled 2-layer test device (a), and shows a cross-sectional image of a single blood-gas bilayer (b). The test devices were made from 2.5 mm thick PDMS pieces and were stacked vascular-to-vascular, in order to better test the gas transfer from one oxygen channel to one vascular channel through the membrane. In devices designed for clinical applications, shown schematically in Fig. 4(a), each vascular layer will lie between two oxygen layers, which will increase the amount of oxygen transferred into each vascular channel.

2.3 Testing the device

Oxygen permeance through the thin membrane of each bilayer was demonstrated by two different methods. The first set of tests was performed to characterize the permeance of the PDMS membrane as a function of both the membrane thickness and the transmembrane pressure, into a static medium. The second set of experiments aimed to quantify the oxygen transfer through the membrane into a flowing liquid medium in the vascular network.

2.3.1 Gas transfer into static medium

The membrane permeance tests were performed with a protocol modeled after similar tests performed by Burgess et al (2008). A supply of oxygen was attached to the vascular channel inlet at a pre-determined pressure. The vascular outlet remained open as the vascular networks were filled with oxygen, while both gas channel inlet and outlet were clamped shut. After the vascular channels were purged with oxygen for 1–2 min, the vascular outlet was closed off using a 3-way stopcock, and the gas channel outlet was unclamped and submerged in water. Oxygen was

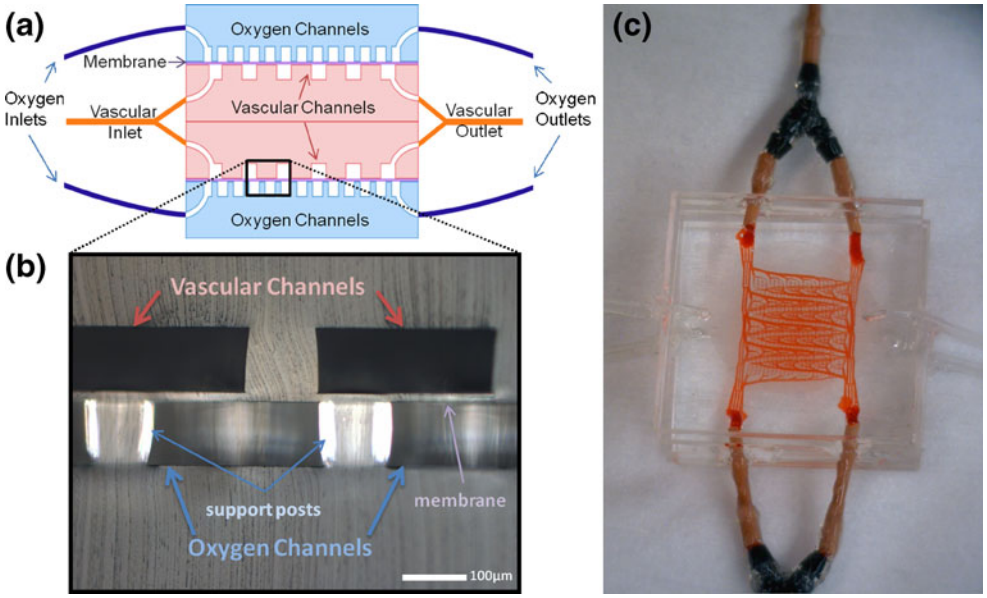

Fig. 3 (**a**) A schematic of the cross section of a test device, built with two bilayers stacked in a vascular-to-vascular configuration to eliminate extra oxygen transfer from the ambient environment or adjacent bilayers. (**b**) A microscope image of the cross section of an individual bilayer shows vascular channels on top, above a PDMS membrane of about 10 μm, and an oxygen channel below, supported by 100 μm posts. (**c**) A photograph of a test device with dyed DI water in the vascular channels, stacked inversely on top of one another for oxygen permeance testing

then permitted to flow through the membrane and out of the device via the gas channel outlet, where a bubble would form in the water. A stopwatch was used to determine the time required for each bubble to form, and the average time of formation was used to determine the oxygen flow rate, (Q_1), based on the estimated bubble volume. Repeated observations suggested that the bubbles were of a constant volume and spherical in shape, with a diameter estimated by visual comparison with reference spheres of known size. This experiment was performed for test devices containing 11, 26, 46, 59, 83, and 120 μm thick membranes, at oxygen inlet pressures of 5 and 10 psig. Each test was run for several minutes to gather enough data for at least 4 bubbles to ensure consistency.

2.3.2 Gas transfer into flowing medium

To assess the rate of oxygen transfer through the membrane into a flowing liquid medium in the vascular network, a second set of oxygenation tests was conducted using a blood gas analyzer. These tests were performed on Phosphate Buffered Saline (PBS) (Invitrogen, Carlsbad, CA) which was initially depleted of oxygen by de-aeration in a vacuum environment for over 12 h. Though oxygenation into PBS is greatly reduced versus oxygenation into blood due to the lack of hemoglobin binding, we aimed to generate an initial model that evaluated the permeance of the PDMS membrane based on the quantity of dissolved oxygen transferred to the PBS. Prior to flow testing, each device

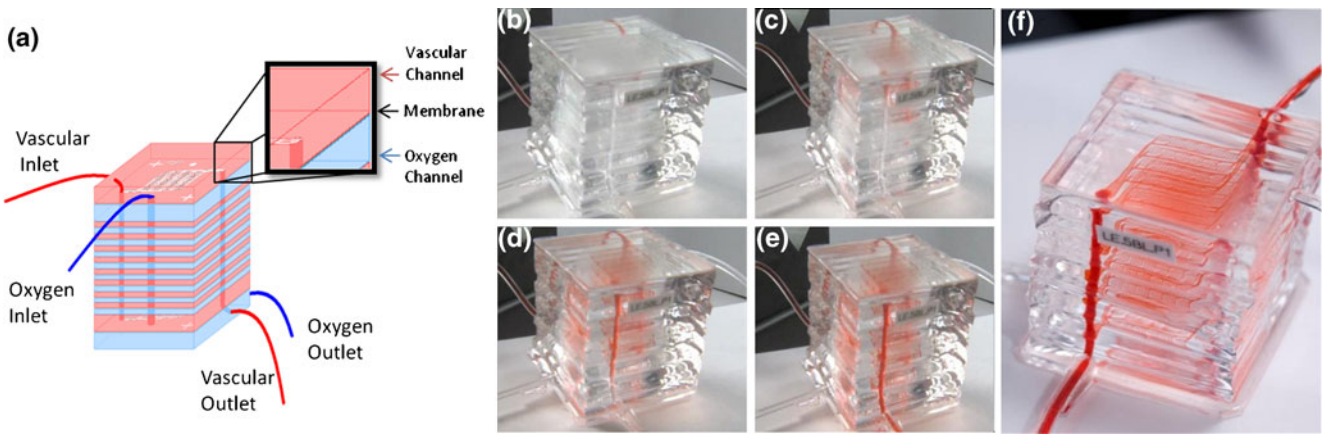

Fig. 4 (**a**) The schematic shows a 10-bilayer device with a cutout of the individual bilayer subunit structure. (**b**–**f**) A 5-bilayer device being filled with dyed DI water at 0.5 mL/min. Device filling starts at t=0 s, and the dye is seen entering the device from the vascular inlet in the back (**b**). The dye is seen flowing through the middle vascular layers at t=4 s (**c**), and t=8 s (**d**). At t=10 s, the device is completely and uniformly filled with the red dye (**e**), showing even fluid distribution throughout each of the 5 vascular networks. (**f**) An alternate view showing the filled vascular channels stacked between oxygen channels

was inspected for flow consistency by filling the vascular channels with DI water containing food coloring for visual clarity. This test was performed on each vascular layer to ensure that there were no blockages, leaks in the membrane, or delamination of the membrane from the walls of the channels. The devices were also primed with deoxygenated PBS, and checked for absence of bubbles before any experiments were run.

A clinical blood gas analyzer (BGA) (Instrumentation Laboratory, Bedford, MA) was used to test the dissolved oxygen before and after each experiment. The base partial pressure of dissolved oxygen (pO_2) of the oxygen-depleted PBS was measured before each experiment was performed. A syringe containing deoxygenated PBS was attached to the vascular inlet tubing of a primed device and flow was administered using a Harvard syringe pump (Harvard Apparatus, Holliston, MA). The device was purged with 1 mL of deoxygenated PBS; flowing oxygen was then administered to the oxygen channel through the inlet at 5 psig. After the device was allowed to reach steady state, and all visual inspections confirmed the absence of any bubbles or leaks within the device, a sample was collected from the vascular outlet. A 2 mL sample of oxygenated PBS was collected using another Harvard syringe pump on the outlet vascular tubing, drawing in the oxygenated PBS at the same rate that the inlet syringe was pushing the deoxygenated PBS through. After an adequate sample was obtained, flow into the device was stopped and the pO_2 was tested for the oxygenated PBS sample. At the end of each experiment, the pO_2 was also tested in the inlet syringe to baseline passive gas transfer in the syringe. The same tests were performed using house air, (21% oxygen), and nitrogen (<0.001% oxygen) instead of oxygen for comparison.

3 Results and discussion

3.1 Fabrication

The device design enabled uniform flow of the test PBS solution through biomimetic microchannels while oxygenating the media through a thin PDMS membrane. Use of the PDMS elastomer enabled easy fabrication and reproduction of a robust device with an ultrathin non-porous membrane. Several devices were built comprising 3, 5 or 10 bilayers alternating in order between oxygen channel and vascular channel, and initial flow testing demonstrated that the fabrication process produced a high yield. A 5-layer stacked device being filled with red DI water and the uniform fluid distribution that the biomimetic vascular network creates are also depicted in Fig. 4(b–f). Over 30 test devices were built and tested; each was capable of holding up to 15 psig gas-side pressure and PBS flow rates up to 10 mL/min. Most of the experiments were performed with a gas inlet pressure of 5 psig, and showed that the 11 μm membranes were able to withstand pressures higher than necessary for ECMO applications. Additional dye testing was done post-experimentation to verify no damage or leaks were caused by the tests.

3.2 Oxygen transfer

3.2.1 Oxygen permeance of the PDMS membrane

The permeance of the membrane as a function of membrane thickness was first examined in static test devices. The results of these experiments summarized in Fig. 5, demonstrate that as the membrane becomes thinner, the permeance increases in the expected manner. To model this relationship, the permeance (K) was found for each test device, according to Eq. 2:

$$K = \frac{Q_2}{SA \cdot \Delta P} \tag{2}$$

Here, the surface area of oxygen transfer (SA) for each device was the same. To adhere to the permeation equation conditions set forth by Yasuda (1975), Q_2 is defined as the actual oxygen flow rate (Q_1) corrected for standard temperature and pressure. The experiments outlined were performed at transmembrane pressures (ΔP) that were estimated at either 5 psig or 10 psig oxygen inlet pressure. In accordance with the predicted behavior from Eq. 2, as the transmembrane pressure doubled, the flow rate also doubled, demonstrating that K is relatively constant for each membrane thickness. Permeance values reported in the literature (Burgess et al, 2008) fall on the curve generated

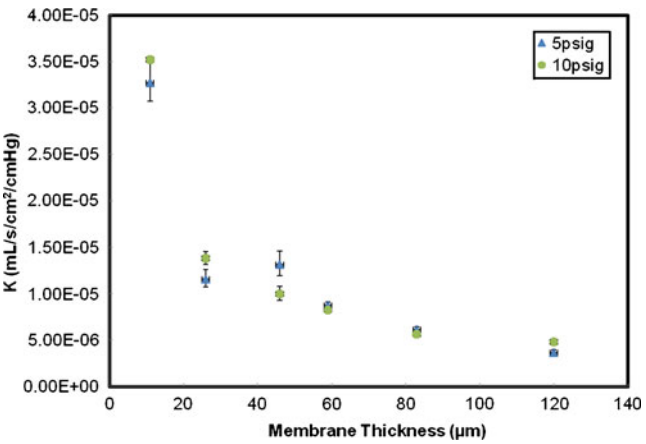

Fig. 5 Oxygen permeance (K) in mL/sec/cm^2/mmHg was plotted against PDMS membrane thickness, in μm, for gas-side inlet pressures of 5 and 10 psig. Data reflects measurements from 4 trials. Error bars represent the standard deviation of bubble formation time, and due to the narrow range may not be visible for some data points

by our experiments for various membrane thicknesses, and confirm the relationship we have developed between the membrane thickness and the oxygen permeability. For the 11 μm membrane that we featured in our devices, the oxygen permeance was observed to be somewhat reduced, averaging roughly 3.5×10^{-5} mL/s/cm^2/cm Hg.

3.2.2 Oxygen transfer into flowing medium

The relationship between gas transfer into flowing PBS and residence time, as assessed by blood gas analysis of PBS, was also investigated. Data from these experiments are plotted for oxygen, house air, and nitrogen gases in Fig. 6. As residence time, defined by the time that a given volume of fluid was in the gas-exchange region of the device, was increased, the oxygen transfer increased as expected. At residence times greater than 1.4 s, the oxygen content in the output PBS exceeded the upper limit of the BGA and was not measurable. At a residence time of 1 s the oxygen content was approximately at a pO_2 of 570 mm Hg, which is equivalent to 17.1 mL/L according to Eq. 3 (Marino 1998).

$$Dissolved\ O_2\left(\frac{mL}{L}\right) = 0.03 \times pO_2 \tag{3}$$

The data shown in Fig. 6 represents an initial investigation of oxygen transfer in a dynamic system, which mimics the flow configuration of a blood oxygenator. Simple analysis of oxygen permeance such as provided by the bubble transfer experiment is not possible in this dynamic situation, due to the presence of several complicating factors. In varying the PBS flow rates and the oxygen composition of the gas used, we observed the transfer of oxygen across the PDMS membrane into a flowing medium, aimed towards understanding the effects of flow on the overall transfer. As membrane thickness was reduced, the oxygen volume transferred was increased, but not in direct inverse proportion as seen in the static experiments. These findings suggest several complicating factors influencing gas transfer in the dynamic system, none of which are accounted for in the simple analysis used to examine the static system in the first set of experiments. These factors include variations in the dissolved oxygen concentration gradient, boundary layer effects influencing oxygen distribution in the fluid channel, complex fluid mechanical effects controlling the actual transmembrane pressure in a dynamic flow environment, and deformation of the membrane due to pressure variations from the gas side to the fluid side. Because of the numerous dynamic factors that a flow system introduces, the gas exchange seen in a static system cannot provide a complete model of gas exchange into flowing medium. The flow tests allowed us to see the difference of gas transfer into a flowing channel, and enables observation of the variation in oxygen transfer that is attributed to the dynamic effects. These effects are the subject of continued investigation, using tools such as computational fluid dynamic models, towards a better understanding of the design considerations and performance characteristics of microfluidic lung oxygenators.

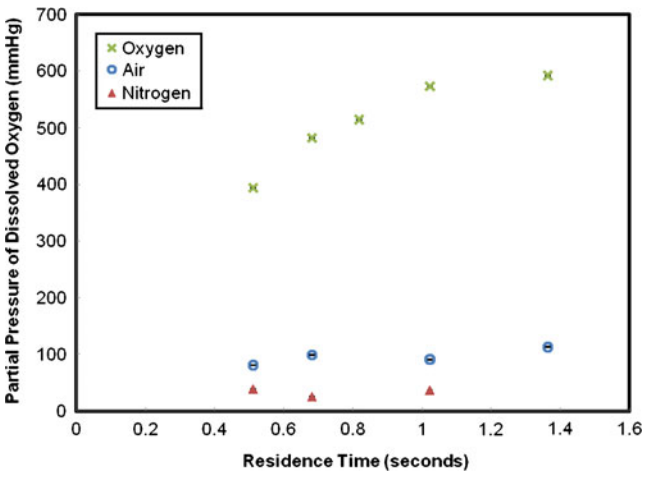

Fig. 6 Partial pressure of oxygen dissolved in PBS as a function of residence time for oxygen (99.99% oxygen content), house air (21% oxygen content) and nitrogen (0% oxygen content) used as the working gas. Each experiment was run with a consistent gas side pressure of 5 psig. The error bars represent the error in the BGA reading, which is 1 mm Hg, and may not be visible due to marker size

4 Conclusion

The microfluidic oxygenator device reported here has shown through initial testing that it is capable of high oxygen transfer rates consistent with the use of ultrathin membranes. The multiple stacked blood-gas bilayer subunits that comprise these devices can be easily and consistently reproduced, and connected in multiple configurations. By stacking the bilayer, we can create oxygenation devices that scale readily for human clinical applications. The membrane thickness in these devices can be controlled over a wide range, and optimized for mechanical and diffusion properties. Furthermore, by making the bilayer subunits out of thinner PDMS sheets, we can create channels that experience gas infusion from the oxygen channel of an adjacent bilayer, increasing overall oxygen transfer. Incorporation of these features will enable this system to move towards the goal of mimicking the alveolar-capillary architecture of the human lung.

The permeance of PDMS membranes provides levels of oxygen transfer consistent with model predictions, as demonstrated in static testing. Gas exchange across the membrane varies with the thickness of the membrane, and is different for static and dynamic systems. Since fluid dynamic effects, such as boundary layer formation and

concentration gradients, influence oxygen transfer significantly, additional computational modeling will be required to fully characterize the device performance under flow. Though the dynamic conditions in this device are not yet fully understood, preliminary flow tests with PBS indicate that with a thin membrane, highly efficient oxygen transfer into the working fluid occurs. Ultimately these microvascular network constructs with thin membranes will be useful in artificial lung applications requiring high transfer rates with minimal blood damage.

References

J. T. Borenstein, MRS Symposium Proceedings 1139, #1139-GG02-01 (2009).

J.T. Borenstein, H. Terai, K.R. King, E.J. Weinberg, M.R. Kaazempur-Mofrad, J.P. Vacanti, Biomed Microdevices **4**, 167 (2002)

J.T. Borenstein, M. Tupper, P. Mack, E. Weinberg, A. Khalil, J. Hsiao, G. García-Cardeña, Biomed Microdevices **12**, 71 (2010)

A. Brand, ISBT Sci Ser **4**, 208 (2009)

K.A. Burgess, H. Hu, W.R. Wagner, W.J. Federspiel, Biomed Microdevices **11**, 117 (2008)

J.P. Camp, T. Stokol, M.L. Shuler, Biomed Microdevices **10**, 179–186 (2008)

K.E. Cook, J. Maxhimer, D.J. Leonard, C. Mavroudis, C.L. Backer, L. F. Mockros, ASAIO J **48**, 620 (2002)

P.W. Dierickx, D.S. De Wachter, F. De Somer, G. Van Nooten, P.R. Verdonck, ASAIO J **47**, 628 (2001)

D.R. Emerson, K. Cieslicki, X. Gu, R.W. Barber, Lab Chip **6**, 447 (2006)

W.J. Federspiel, K.A. Henchir, in *Encyclopedia of Biomater and Biomedical Eng*, ed. by G.E. Wnek, G.L. Bowlin (Marcel Dekker, New York, 2004), pp. 922–931

J.W. Hammon, in *Cardiac Surgery in the Adult*, ed. by L.H. Cohn (McGraw-Hill, New York, 2008), pp. 350–370

B. G. Hattler, W.J. Federspiel, in *Gas Exchange in the Venous System: Support for the Failing Lung*, ed. by S.N. Vaslef, R.W. Anderson. (The Artificial Lung: Landes Bioscience, 2002), p. 133–174

K.M. High, M.T. Snider, G. Bashein, in *Cardiopulmonary Bypass Principles and Practice*, ed. by G.P. Gravlee, R.F. Davis, M. Kurusz, J.R. Utley (Williams & Wilkins, Philadelphia, 2000), pp. 28–54

D. Huh, B.D. Matthews, A. Mammoto, M. Montoya-Zavala, H.Y. Hsin, D.E. Ingber, Science **328**, 1662 (2010)

E. Leclerc, Y. Sakai, T. Fujii, Biomed Microdevices **5**, 109 (2003)

J.K. Lee, H.H. Kung, L.F. Mockros, ASAIO J **54**, 372 (2008)

L.B. Leverett, J.D. Hellums, C.P. Alfrey, E.C. Lynch, Biophys J **12**, 257 (1972)

D. Lim, Y. Kamotani, B. Cho, J. Mazumder, S. Takayama, Lab Chip **3**, 318 (2003)

P.L. Marino, in *The ICU Book*, ed. by B. Brown, N. Dernoski, T. Lazar (Lippincott Williams & Wilkins, Philadelphia, 1998), p. 21

L. F. Mockros, K. E. Cook, in *The Artificial Lung (Tissue Engineering Intelligence Unit 7*, ed. By S.N. Vaslef, R.W. Anderson, (Landes Bioscience, Austin, 2002), p. 33

J.P. Montoya, C.J. Shanley, S.I. Merz, R.H. Bartlett, ASAIO J **38**, M399–M405 (1992)

C.D. Murray, Proc Natl Acad Sci **12**, 299 (1926)

Y. Niimi, K. Ueyama, K. Yamaji, S. Yamane, E. Tayama, A. Sueoka, K. Kuwana, K. Tahara, Y. Nosé, Artif Organs **21**, 1082 (1997)

T.C. Page, C.B. McKay, W.R. Light, J.D. Hellums, in *Blood Substitutes*, ed. by R.M. Winslow, K.D. Vandegriff, M. Intaglietta (Birkhauser, Boston, 1996), pp. 132–145

T.C. Page, W.R. Light, J.D. Hellums, in *Oxygen transport to tissue XXI*, ed. by A. Eke, D. Deply (Kluwer Academic/Plenum Publishers, New York, 1999), pp. 715–730

C.T. Seo, C.H. Bae, D.S. Eun, J.K. Shin, J.H. Lee, Jpn J Appl Phys **43**, 7773 (2004)

T. Shimono, Y. Shomura, I. Hioki, A. Shimamoto, H. Tenpaku, Y. Maze, K. Onoda, M. Takao, H. Shimpo, I. Yada, Ann Thorac Surg **63**, 1730 (1997)

B. Stiller, J. Lemmer, F. Merkle, V. Alexi-Meskishvili, Y. Weng, M. Hübler, A. Koster, T. Drews, P.E. Lange, R. Hetzer, Intensive Care Med **30**, 1814 (2004)

G.J. Wang, K.H. Ho, S.H. Hsu, K.P. Wang, Biomed Microdevices **9**, 657 (2007)

E. J. Weinberg, J. T. Borenstein, M. R. Kaazempur-Mofrad, B. Orrick, J. P. Vacanti, MRS Symposium Proceedings. MRS Press **820**, 121 (2004)

H. Yasuda, J Appl Polym Sci **19**, 2529 (1975)